Letters

Full Integration of On-Board Charger, Auxiliary Power Module, and Wireless Charger for Electric Vehicles Using Multipurpose Magnetic Couplers

Ziwei Liang, *Graduate Student Member, IEEE*, Liyan Zhu, *Member, IEEE*, Yue Sun, *Graduate Student Member, IEEE*, Jie Li, *Member, IEEE*, Ruiyang Qin, *Member, IEEE*, Basu Arka, *Graduate Student Member, IEEE*, Daniel Costinett, *Senior Member, IEEE*, and Hua Bai, *Senior Member, IEEE*

***Abstract*—To further improve the system integration and convenience of the battery charging system for electric vehicles, this letter proposed a multipurpose magnetic coupler-based charging solution that integrates bidirectional on-board charger (OBC), wireless power transfer (WPT), and an auxiliary power module (APM). The proposed solution presents multiple highlights: 1) the first exhibited solution to integrate OBC, WPT, and APM in one unit; 2) magnetic integration that uses a multiwinding WPT pad to eliminate the main transformer of OBC and APM; and 3) topological integration that saves multiple active and passive devices. This letter includes a description of the system topology, operation principles of individual charging modes, a novel magnetic coupler, and the design methodology. Finally, a prototype was constructed and different charging modes were tested to validate the proposed design.**

***Index Terms*—Battery chargers, electric vehicles (EVs), integrated magnetics, multiport converters, wireless power transfer (WPT).**

I. Introduction

ADVANCED charging systems are essential for promoting the adoption of electric vehicles (EVs), as they help to alleviate mileage anxiety and enhance the user experience [1]. To offer more convenience than conductive charging, the automotive industry is also exploring wireless power transfer (WPT)-based charging solutions, which provide a hassle-free charging experience but are usually expensive with limited charging power. EVs equipped with both on-board charger (OBC) and WPT allow users to select either charging speed or charging convenience but could be bulky and costly.

In addition, the auxiliary power module (APM) is an inevitable on-board unit that charges the 12 V battery to support low voltage (LV) loads on vehicles. Usually, OBC, WPT, and APM are designed, manufactured, and installed separately. This requires a complex cooling system, complicated assembly, and eventually high cost and large size. To improve the power density and reduce the cost of charging units, different levels of the integration of charging units have been proposed in past decades [2], [3], [4], [5], [6], [7].

Mechanical integration is a basic and low-level integration, which can help to increase the system's compactness, however, only saves the cost of the enclosure and cooling system. High-level topological and magnetical integration is much more preferred for next-generation integrated charging systems. In [3], a dual-transformer topology is utilized to integrate OBC and APM by sharing the rectifier. The integration is further improved by using a three-port transformer to build a voltage-fed (VF) triple-active bridge [4] or a current-fed (CF) triple-active bridge [5]. Similarly, the integration of OBC and WPT has been realized by sharing an active bridge [6]. Recently, high-level integration of OBC and WPT with the shared full bridge and magnetic components is presented in [7]. However, using the aforementioned integration approaches, at least two separate units are still needed for EVs that intend to offer both conductive and wireless charging methods at the same time.

To achieve a higher-level integration of the EV charging system, a full integration of bidirectional OBC, WPT, and APM using a multipurpose magnetic coupler is proposed in this letter, which is inspired by previously successful integration cases, i.e., OBC+APM and OBC+WPT. Figs. 1 and 2 show the block diagram of the conventional standalone solution and the proposed integrated solution, respectively. Compared with the standalone solution and the previous integrated chargers, the proposed integration method offers several benefits: 1) integration of OBC, WPT, and APM by one compact unit

Manuscript received 5 June 2023; revised 5 October 2023; accepted 27 October 2023. *(Corresponding author: Liyan Zhu.)*

The authors are with the Department of Electrical Engineering and Computer Science, University of Tennessee—Knoxville, College of Engineering, Knoxville, TN 37916 USA (e-mail: zliang7@vols.utk.edu; liyanz@vt.edu; ysun79@vols.utk.edu; jli94@vols.utk.edu; rqin1@alum.utk.edu; abasu1@vols.utk.edu; daniel.costinett@utk.edu; hbai2@utk.edu).

Color versions of one or more figures in this article are available at https://doi.org/10.1109/TIE.2023.3331082.

Digital Object Identifier 10.1109/TIE.2023.3331082

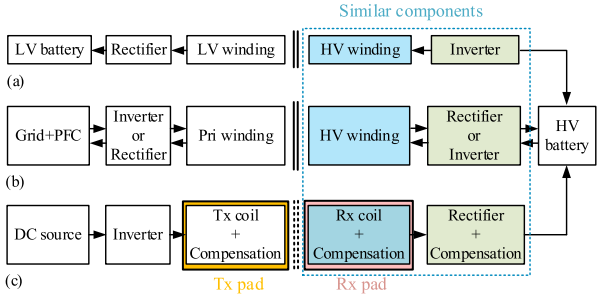

Fig. 1. Block diagram of the EV charging system with standalone OBC, WPT, and APM units. (a) APM. (b) OBC. (c) WPT.

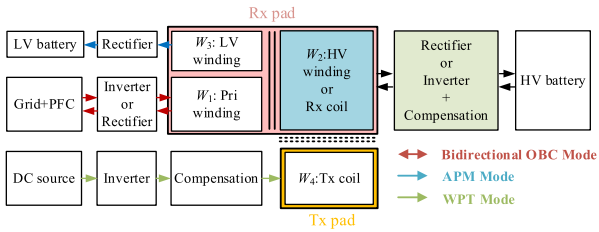

Fig. 2. Block diagram of the proposed fully integrated EV charging system with the OBC, APM, and WPT functions using multipurpose magnetic coupler and shared circuit components.

through a simple multipurpose magnetic coupler and 2) elimination of two HV active bridges, two conventional transformers and other related active and passive components in the standalone units. The EV charging system can then achieve higher power density and lower cost.

II. Proposed Integration Method

A. Topology

The proposed integrated EV charger is shown in Fig. 3. Coils W_1–W_4 form a multipurpose magnetic coupler, where W_2 is shared and can serve as the secondary winding of the OBC, the receiver (Rx) coil of the WPT, and the primary winding of the APM. To connect to the 3-Φ grid with up to 480 Vac line-line voltage and generate the dc bus voltage up to 800 V, a multilevel topology is adopted aiming at using lower-voltage power switches. Here, Q_{a1}–Q_{a6} form a three-level (3-L) active-neutral-point-clamp phase leg, and 3-Φ legs form the complete ac–dc stage. P_1–P_4, S_{11}–S_{14}, and S_{31}–S_{34} form a triple-active-bridge (TAB) converter with a VF port at the HV side and a CF port at the LV side. S_{21}–S_{24} form a 3-L dc/dc converter at HV side, which connects to the 400 V/800 V battery. S_{41}–S_{44} form the WPT inverter. C_b is the dc blocking cap, L_{o1} is the inductor of the dc/dc converter for the OBC and the WPT, and L_{o2}–L_{o3} is the coupled filter inductor for the APM. The inductor-capacitor-capacitor-series compensation topology, which consists of L_{r1}, C_{r1}, C_{r2}, and C_{r3}, is adopted for WPT.

B. Operation Mode

When the system works in the OBC mode or the APM mode, The operation frequency is much higher than the resonant frequency of the WPT mode, thus the impedance of C_b and Cr_3 can be ignored, and the charger is operated as a TAB converter. The three-port transformer consists of closely coupled W_1, W_2, and W_3. Phase-shift modulation and pulsewidth modulation can be used to decouple the power flow and modulate the output power [5], [8]. The output power can be regulated by TAB and the following dc/dc stage.

In WPT mode, the converter is working at the resonant frequency, which is calculated as follows:

$$2\pi f_{\text{WPT}} = \frac{1}{\sqrt{L_2 C_{r3}}} = \frac{1}{\sqrt{L_{r1} C_{r2}}} = \frac{1}{\sqrt{L_4 \frac{C_{r1} C_{r2}}{C_{r1}+C_{r2}}}}. \quad (1)$$

The zero-current-detection-based synchronized rectifier control is utilized at the Rx side to improve efficiency [9]. To avoid impacts of the induced voltage on W_2 and W_3, relay K_{pri} and K_{lv} will be open in the WPT mode WPT.

III. Magnetic Coupler Design

The structure of the proposed magnetic coupler is shown in Fig. 4, with coils W_1, W_2, and W_3 forming a strongly coupled three-winding transformer for OBC and APM modes, while W_2 is loosely coupled with W_4 for the WPT mode.

The design method of the proposed magnetic coupler is summarized in Fig. 5. Because the magnetic coupler is derived from the conventional WPT pad, the design procedure is: 1) WPT Rx and Tx coil, W_2 and W_4, 2) OBC primary coil, W_1, and 3) LV secondary coil, W_3. The basic design principles are introduced as follows.

As of W_2 and W_4 for the WPT, higher coupling coefficient k and quality factor Q are always preferred when designing Rx and transmitter (Tx) coils for high efficiency and high power. The main factors that affect k and Q of coils are: 1) Coil size, 2) Coil topology, 3) Coil turns, and 4) Materials of the ferrite tiles and wires. Considering the flexibility of integrating other coils in the Rx pad, the most common circular planar topology is chosen and the outer diameter is set to 500 mm to transfer 6.6 kW efficiently with 200 mm vertical distance [10], [11].

To integrate W_1 and W_3 into the Rx pad, all windings are designed to the same planar form as W_2. For W_1 and W_3, the main design variables are the leakage inductance and the turn ratio. Considering the rated voltage range at the primary side, HV side, and LV side is 300–400 V, 250–450 V, and 20–50 V, respectively, the turn radio of W_1, W_2, and W_3 is set to 14:14:1. To fully utilize the space and ferrite tiles of the Rx pad and ensure strong coupling, the interleaved structure is applied, as shown in Fig. 4.

Different from the conventional transformer, adding one single LV turn will lead to low coupling between coils, and thick wire is needed considering the high-current capability. To reduce the resistance of the LV coil and achieve strong coupling, a multiturn-paralleling structure is used.

Based on the selected Litz wires, the arrangement, i.e., vertical and horizontal arrangements, and the position of LV coil as shown in Fig. 6, are optimized. The paralleling turn number is mainly determined by the RMS current of the LV side. However, too few turns can lead to weak coupling between W_2 and W_3. For the prototype, eight parallelling turns are used for the LV coil.

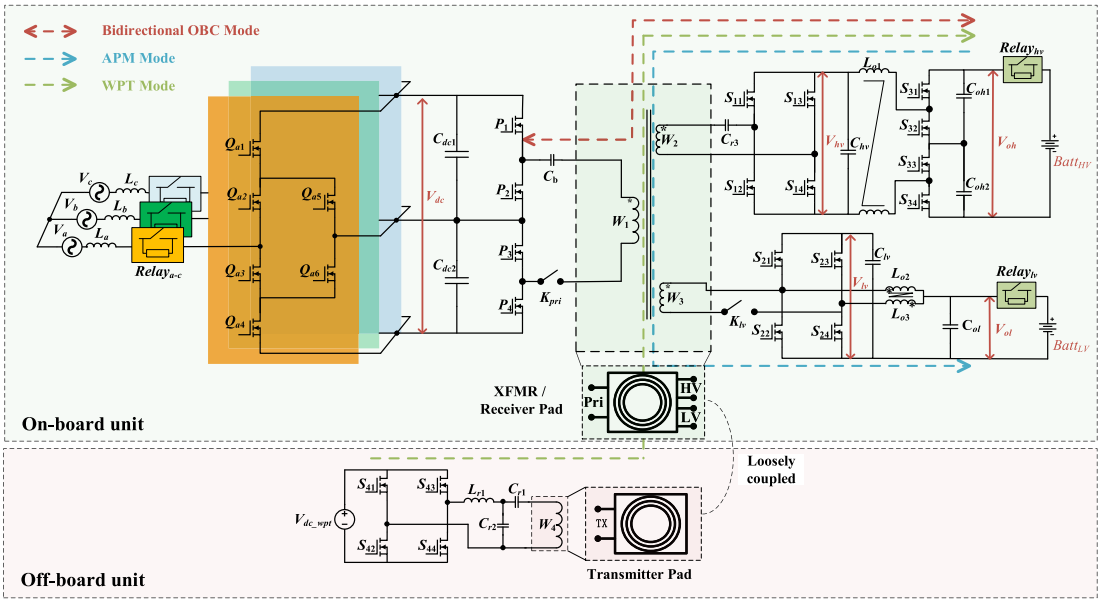

Fig. 3. Proposed topology of the fully integrated EV charger.

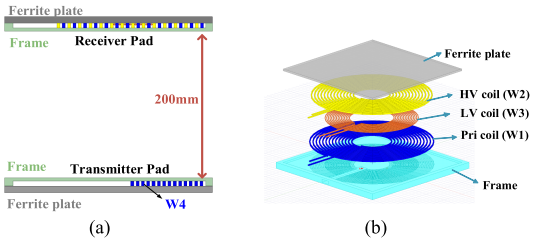

Fig. 4. Charging pads structure. (a) Section view of two pads. (b) Explosive view of the Rx pad.

The simulated coupling coefficient between W_2 and W_3, and the leakage inductance at the LV side are conducted for optimization purpose, as shown in Fig. 7. It shows that the horizontal arrangement has the higher coupling coefficient and the lower leakage inductance. Thereby, the case shown in Fig. 6(d) is used for the prototype.

The advantages of such a design are summarized in the following.

1) The design methodology of conventional WPT coils can still be referenced and utilized.
2) The structure is simple, and the size and thickness of the pad are not increased with three coils integrated in.
3) Strong coupling of W_1, W_2, and W_3 can be ensured, and core loss could be much smaller than using the conventional transformer, benefiting from the larger ferrite tile size.

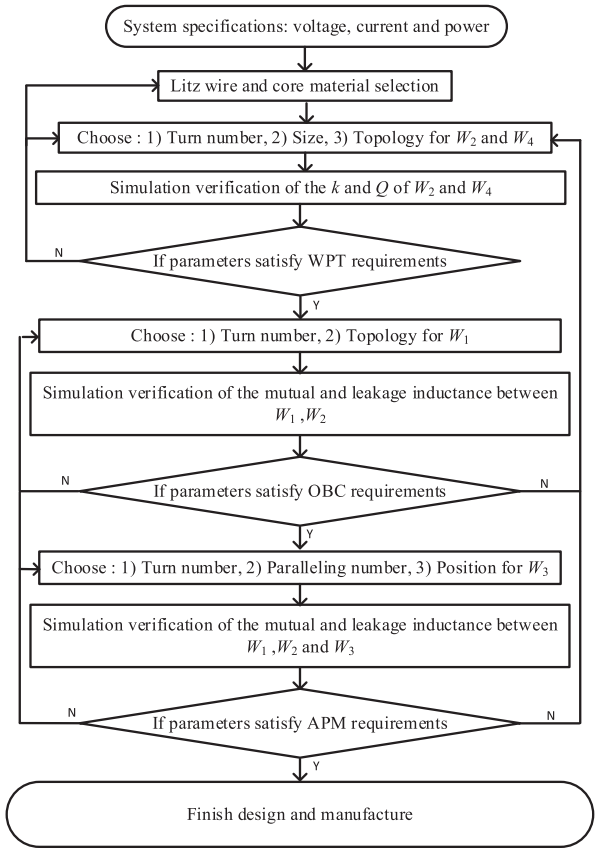

Fig. 5. Design method of the proposed magnetic coupler.

IV. Simulation and Experimental Validation

As shown in Fig. 8, the magnetic coupler is manufactured. The specifications of the proposed magnetic coupler are listed in Table I. The measured parameters of the coupler are shown in Table II , where k_{12}, k_{23}, and k_{24} are the coupling coefficients of the respective coils. k_{24} is measured with a 200 mm air gap between two pads. Large k_{12} reflects the strong coupling resulting

Fig. 6. Examples of the LV coils with different arrangements and positions. (a) Vertical, LV position = 0. (b) Vertical, LV position = 10. (c) Horizontal, LV position = 0. (d) Horizontal, LV position = 10.

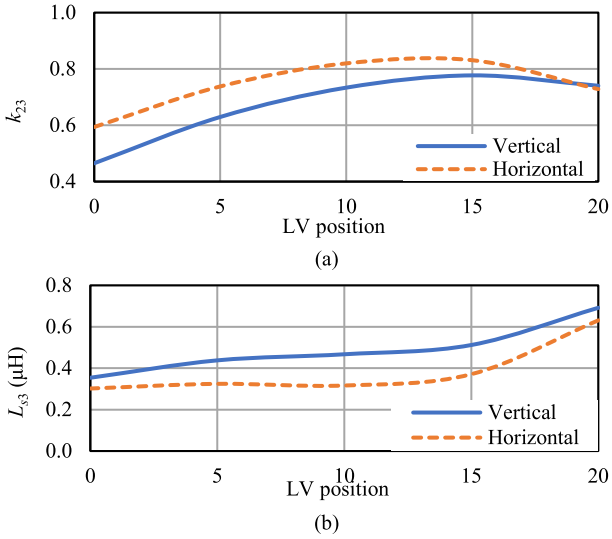

Fig. 7. Simulation results based on the eight-turn paralleled LV coil. (a) Coupling coefficient between HV and LV coils. (b) Leakage inductance on LV side.

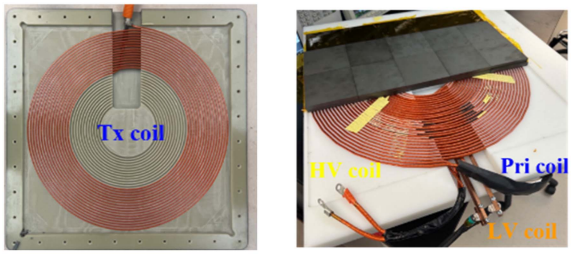

Fig. 8. Manufactured pads. (a) Tx pad. (b) Rx pad.

TABLE I
SPECIFICATIONS OF THE MAGNETIC COUPLER

Coil	Pri coil (W_1)	HV coil (W_2)	Tx coil (W_3)	LV coil (W_4)
Litz wire	NLD3300/42SPPIT (New England wire)			NELD1710/42SPSN (New England wire)
Size (mm)	5.89 × 3.56			⌀ 2.87
Equiv. AWG	4			12
Outer diameter (mm)	480	464	480	176.8
Inner diameter (mm)	69.5	63.1	145.8	132.9
Magnetic tile	FPL100/100/4-BH1T			

TABLE II
PARAMETERS OF THE MAGNETIC COUPLER

Parameter	L_1	L_2	L_3	L_4	L_{s1}
Value	90.3 μH	86 μH	1.47 μH	212 μH	5.23 μH
Parameter	L_{s2}	L_{s3}	k_{12}	k_{23}	k_{24}
Value	1.58 μH	0.31 μH	0.95	0.66	0.133

TABLE III
SYSTEM SPECIFICATIONS

Parameter	f_{OBC}	f_{APM}	f_{WPT}	L_{r1}	C_{r1}	C_{r2}
Value	240 kHz	100 kHz	42.5 kHz	63.3 μH	85 nF	250 nF
Parameter	C_{r3}	V_{ac}	V_{dcbus}	V_{dc_WPT}	V_{bat_HV}	V_{bat_LV}
Value	176 nF	380 V	650 V	400 V	350 V	12 V

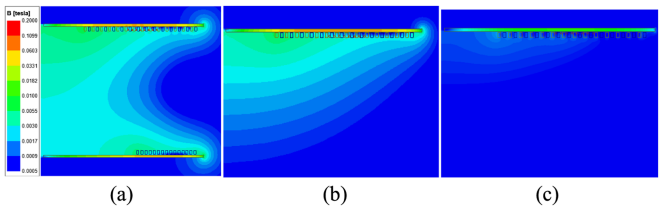

Fig. 9. Simulated flux density distribution. (a) WPT. (b) OBC. (c) APM.

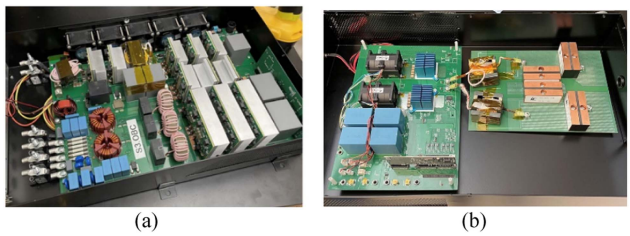

Fig. 10. Experimental prototype. (a) On-board unit. (b) Off-board unit.

from the interleaved design. k_{12} and k_{24} are also acceptable for APM and WPT systems. The system specifications are given in Table III.

The simulated magnetic field in the tiles and air space at OBC, APM, and WPT modes is shown in Fig. 9. Maximum magnetic flux densities in the ferrite tiles are 0.08 T, 0.012 T, and 0.013 T for 6.6 kW WPT, 6.6 kW OBC, and 1.5 kW APM, respectively. The simulations verify that, in addition to the WPT function, the ferrite tiles in the proposed magnetic coupler also satisfy the requirement of OBC and APM modes. No additional cores or separate transformers are needed, which is aligned with the analysis in Section III and lower core loss in the OBC and APM mode can be expected.

A prototype, including the on-board unit and off-board unit, is built, as shown in Fig. 10. All individual functions are verified by experiments, including 10.3 kW OBC, 6.6 kW WPT, 3.7 kW vehicle-to-load (V2L), and 800 W APM. A battery emulator is used as the load for the OBC, WPT, and APM test, and a fixed three-phase resistive load of 22 Ω on each phase is used for the V2L mode. The key waveforms are shown in Fig. 11, and the measured efficiency curves are shown in Fig. 12. Peak efficiency of 96.1%, 92%, and 92% are achieved for bidirectional

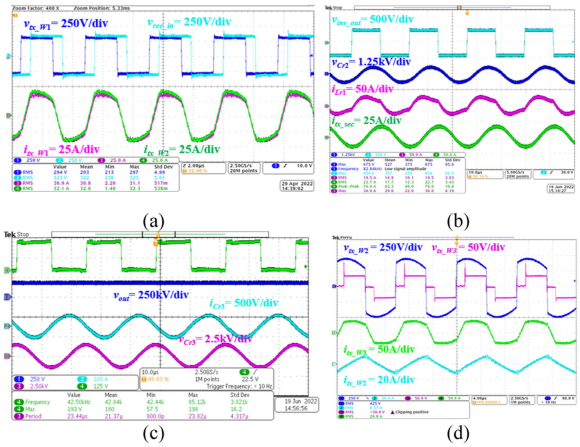

Fig. 11. Key waveforms. (a) OBC. (b) WPT inverter. (c) WPT secondary sync rectifier. (d) APM mode.

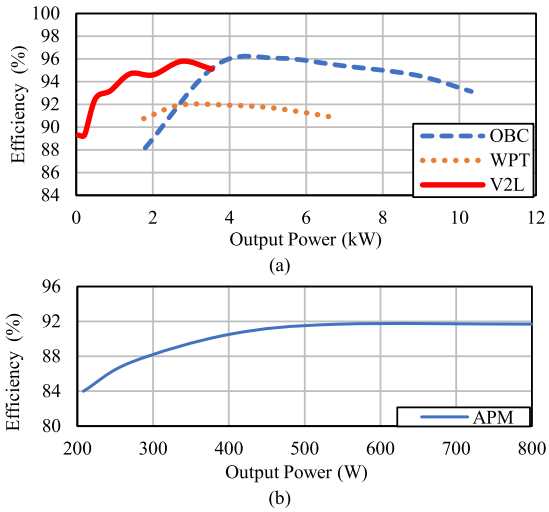

Fig. 12. Efficiency of different modes. (a) OBC, WPT, and V2L. (b) APM.

OBC, WPT, and APM, respectively. Although, there is still further improvement to make in future work, e.g., increasing the efficiency of WPT and OBC at the light load due to hard switching, nevertheless, all functions are evaluated by the experiments, and the volume of 9.92 L is achieved by the on-board unit of the proposed integrated charger. A comparison between the standalone units and the proposed integrated charger is given in Table IV. Based on the average power density of the reference design, the total volume of the standalone OBC+APM+WPT having a similar power capability is estimated to be >12 L. Therefore, the volume reduction of over 2 L is achieved and a smaller pad is used compared with the references.

V. Conclusion

This letter introduces a novel multipurpose magnetic coupler-based fully integrated charger capable of offering WPT, bidirectional OBC, and APM functionalities within a single unit. By integrating three coils into the Rx pad, it not only serves as the WPT mode's Rx pad but also functions as the three-winding transformer for the TAB converter in both OBC and APM modes. Despite its multifunctionality, the Rx pad retains a simple and compact design. When compared with standalone solutions, the proposed integrated system eliminates the need for two traditional transformers and two active bridges. This results in a >2L volume reduction and corresponding cost decreases. Comprehensive evaluations of the proposed functionalities were conducted, with experimental results affirming the efficacy of this integrated approach.

TABLE IV
Comparison of the Standalone Units and the Proposed Integrated Charger

	OBC [12],[13],[14]	APM [15],[16],[17]	WPT [18],[19],[20]	This work
Average power density (kW/L)	1.29	0.45	–	1.85
Average pad size (m^2)	N/A	N/A	0.42	0.2
Total volume of 11kW OBC+ 0.8kW APM + 6.6kW WPT	> 12 L			9.92 L

References

[1] H. K. Bai et al., "Charging electric vehicle batteries: Wired and wireless power transfer: Exploring EV charging technologies," *IEEE Power Electron. Mag.*, vol. 9, no. 2, pp. 14–29, Jun. 2022, doi: 10.1109/MPEL.2022.3173543.

[2] M. Y. Metwly, M. S. Abdel-Majeed, A. S. Abdel-Khalik, R. A. Hamdy, M. S. Hamad, and S. Ahmed, "A review of integrated on-board EV battery chargers: Advanced topologies, recent developments and optimal selection of FSCW slot/pole combination," *IEEE Access*, vol. 8, pp. 85216–85242, 2020, doi: 10.1109/ACCESS.2020.2992741.

[3] G. Yu and S. Choi, "An effective integration of APM and OBC with simultaneous operation and entire ZVS range for electric vehicle," *IEEE Trans. Power Electron.*, vol. 36, no. 9, pp. 10343–10354, Sep. 2021, doi: 10.1109/TPEL.2021.3063931.

[4] I. Kougioulis, P. Wheeler, and M. R. Ahmed, "An integrated on-board charger and auxiliary power module for electric vehicles," in *Proc. IEEE Appl. Power Electron. Conf. Expo.*, 2022, pp. 1162–1169, doi: 10.1109/APEC43599.2022.9773777.

[5] L. Zhu, H. Bai, A. Brown, and L. Keuck, "A current-fed three-port DC/DC converter for integration of on-board charger and auxiliary power module in electric vehicles," in *Proc. IEEE Appl. Power Electron. Conf. Expo.*, 2021, pp. 577–582, doi: 10.1109/APEC42165.2021.9487263.

[6] M. Elshaer, C. Bell, A. Hamid, and J. Wang, "DC–DC topology for interfacing a wireless power transfer system to an on-board conductive charger for plug-in electric vehicles," *IEEE Trans. Ind. Appl.*, vol. 57, no. 6, pp. 5552–5561, Nov./Dec. 2021, doi: 10.1109/TIA.2021.3103700.

[7] Y. Zhang et al., "Integration of onboard charger and wireless charging system for electric vehicles with shared coupler, compensation, and rectifier," *IEEE Trans. Ind. Electron.*, vol. 70, no. 7, pp. 7511–7514, Jul. 2023, doi: 10.1109/TIE.2022.3204857.

[8] Y. Yan, H. Bai, A. Foote, and W. Wang, "Securing full-power-range zero-voltage switching in both steady-state and transient operations for a dual-active-bridge-based bidirectional electric vehicle charger," *IEEE Trans. Power Electron.*, vol. 35, no. 7, pp. 7506–7519, Jul. 2020, doi: 10.1109/TPEL.2019.2955896.

[9] S. Cochran and D. Costinett, "Discrete time synchronization modeling for active rectifiers in wireless power transfer systems," in *Proc. 20th Workshop Control Model. Power Electron.*, 2019, pp. 1–8, doi: 10.1109/COMPEL.2019.8769717.

[10] S. Li, F. Li, R. Zhang, C. Tao, and L. Wang, "Accurate modeling, design, and load estimation of LCC-S based WPT system with a wide range of load," *IEEE Trans. Power Electron.*, vol. 38, no. 10, pp. 11763–11775, Oct. 2023, doi: 10.1109/TPEL.2023.3279659.

[11] M. Al-Saadi, A. Ibrahim, A. Al-Omari, A. Al-Gizi, and A. Craciunescu, "Analysis and comparison of resonance topologies in 6.6 kW inductive wireless charging for electric vehicles batteries," *Procedia Manuf.*, vol. 32, pp. 426–433, Jan. 2019, doi: 10.1016/j.promfg.2019.02.236.

[12] "11KW on board charger, OBC," Sinovation Ev, 2021. Accessed: Sep. 28, 2023. [Online]. Available: https://www.sinovation-ev.com/11kw-liquid-cooled-obc

[13] OVAR, "CAD222DF EV on-board charger" 2021. [Online]. Available: https://www.ovartech.com/wp-content/uploads/2021/08/Ovartech-740V-22KW-OBC-Data-Sheet.pdf

[14] "Innolectric_on-board_charger_factsheet_CPS-OBC-E1-2301.pdf," 2023. Accessed: Sep. 28, 2023. [Online]. Available: https://innolectric.ag/wp-content/uploads/2023/01/innolectric_On-Board_Charger_Factsheet_CPS-OBC-E1-2301.pdf

[15] "2KW-DC-to-DC-Converter-VDD202S360-14.pdf," 2017. Accessed: Sep. 28, 2023. [Online]. Available: https://www.ovartech.com/wp-content/uploads/2017/12/2KW-DC-to-DC-Converter-VDD202S360-14.pdf

[16] "China customized 2KW DC/DC converter manufacturers - Grasen," 2019. Accessed: Sep. 28, 2023. [Online]. Available: https://www.grasen-power.com/dc-dc-converter/2kw-dc-dc-converter.html

[17] "Delphi-DCDC-Guide.pdf," 2019. Accessed: Sep. 28, 2023. [Online]. Available: https://stealthev.com/wp-content/uploads/2019/06/Delphi-DCDC-Guide.pdf

[18] S. Li, W. Li, J. Deng, T. D. Nguyen, and C. C. Mi, "A double-sided LCC compensation network and its tuning method for wireless power transfer," *IEEE Trans. Veh. Technol.*, vol. 64, no. 6, pp. 2261–2273, Jun. 2015, doi: 10.1109/TVT.2014.2347006.

[19] S. Moon, B.-C. Kim, S.-Y. Cho, C.-H. Ahn, and G.-W. Moon, "Analysis and design of a wireless power transfer system with an intermediate coil for high efficiency," *IEEE Trans. Ind. Electron.*, vol. 61, no. 11, pp. 5861–5870, Nov. 2014, doi: 10.1109/TIE.2014.2301762.

[20] C. Liu, S. Ge, Y. Guo, H. Li, and G. Cai, "Double-LCL resonant compensation network for electric vehicles wireless power transfer: Experimental study and analysis," *IET Power Electron.*, vol. 9, pp. 2262–2270, Sep. 2016, doi: 10.1049/iet-pel.2015.0186.